Journal of Solid State Chemistry 293 (2021) 121753

Contents lists available at ScienceDirect

Journal of Solid State Chemistry

journal homepage: www.elsevier.com/locate/jssc

Synthesis and luminescent properties of $(RE_{0.95}Ln_{0.05})_2O_2S$ (RE = La, Y; Ln = Ho, Tm)

E.I. Sal'nikova [a,b,*], Yu.G. Denisenko [c], I.E. Kolesnikov [d,e], E. Lähderanta [e], O.V. Andreev [a,f], N.O. Azarapin [a], S.A. Basova [a], A.A. Gubin [g], A.S. Oreshonkov [h,i]

[a] Department of Inorganic and Physical Chemistry, Tyumen State University, Tyumen, 625003, Russia
[b] Komissarov Department of General Chemistry, Northen Trans-Ural Agricultural University, Tyumen, 625003, Russia
[c] Department of General and Special Chemistry, Industrial University of Tyumen, Tyumen, 625000, Russia
[d] Center for Optical and Laser Materials Research, St. Petersburg State University, St. Petersburg, 199034, Russia
[e] Department of Physics, Lappeenranta University of Technology LUT, Lappeenranta, 53850, Finland
[f] Laboratory of the Chemistry of Rare Earth Compounds, Institute of Solid State Chemistry, UB RAS, 620137, Ekaterinburg, Russia
[g] Laboratory of Electron and Probe Microscopy, Tyumen State University, Tyumen, 625003, Russia
[h] Siberian Federal University, Krasnoyarsk, 660041, Russia
[i] Laboratory of Molecular Spectroscopy, Kirensky Institute of Physics Federal Research Center KSC SB RAS, Krasnoyarsk, 660036, Russia

ARTICLE INFO

Keywords:
Rare earth oxysulfides
Synthesis
Rietveld
Luminescence
Lifetime
Quantum yield

ABSTRACT

Solid solutions of oxysulfides $(RE_{0.95}Ln_{0.05})_2O_2S$ (RE = La, Y; Ln = Ho, Tm) were obtained by hydrogen reduction of the co-precipitated sulfates followed by sulfidation of the reaction products. The crystal chemical characteristics of the obtained compounds were refined by the Rietveld method. Morphological certification of particles in the dynamics of synthesis was performed. Most of the particles produced by chemical reactions have a cut that indicates the formation of a compound with a hexagonal syngony with angles of 60 and 120°. This indicates that the thermal effect of gaseous reagents H_2, H_2S on sulfates leads to heterogeneous reactions of thermal dissociation and the formation of new phases. Steady state luminescence properties displayed characteristic sharp bands corresponding to 4f-4f transitions. Luminescence decay curves of all studied samples showed monoexponential decay with microsecond and hundreds microsecond lifetimes depending on doping ions. Calculated color coordinates of Ho^{3+} and Tm^{3+}-doped powders make them promising candidates to be used as phosphors.

1. Introduction

The rare-earth oxysulfides La_2O_2S (La^0 $[Xe]5d^16s^2$), Gd_2O_2S (Gd^0 $[Xe]4f^75d^16s^2$), Y_2O_2S (Y^0 $[Xe]5d^15s^2$), Lu_2O_2S (Lu^0 $[Xe]4f^{14}5d^16s^2$), due to the peculiarities of their electronic structure, can be regarded as unique luminescent structures for practical use and for basic research [1,2]. Luminescence is mainly determined by the nature of the activator ion, but the host matrix into which this ion is embedded affects the intensity of the emission lines through its crystal field [3,4].

Compounds $RE_2O_2S:Ln^{3+}$ are in great demand due to their excellent luminescent properties and color purity [5]. They can be suitable for creating thermographic phosphors (excellent candidates for fluorescence measurements of physiological temperatures using a miniature temperature sensor up to nanoscale) [6]. The authors of [7–12] synthesized and studied the properties of new materials that demonstrate unique thermal and luminescent properties.

Most phosphors are excited by ultraviolet light and exhibit temperature sensitivity, which allows them to be used to control temperature conditions in gas turbine combustion chambers in high-temperature areas of the turbine [13], as well as in X-ray diffraction and scintillation equipment [14]. These materials have the ability to store and release large volumes of oxygen under oxidation/reduction conditions, which makes them interesting as nanocatalysts [15], allows them to be used as laser detection of securities counterfeits [16], to create ultraviolet LEDs (white lamps light) [17], in photovoltaic solar cells [18], as a coating of reinforcing screens during magnetic resonance imaging [19].

Nanophosphors are a class of materials with unique properties that make them very attractive for biological applications [20]. Information about the compositions studied in this paper is rather limited. In Ref. [21], the optical fluorescence of ten trivalent lanthanide ions: Pr^{3+}, Nd^{3+}, Sm^{3+}, Eu^{3+}, Gd^{3+}, Tb^{3+}, Dy^{3+}, Ho^{3+}, Er^{3+}, and Tm^{3+} in Y_2O_2S, La_2O_2S, and Gd_2O_2S matrices, measured using X-ray excitation at 300 K.

* Corresponding author. Department of Inorganic and Physical Chemistry, Tyumen State University, Tyumen, 625003, Russia
E-mail address: elenasalnikova213@gmail.com (E.I. Sal'nikova).

https://doi.org/10.1016/j.jssc.2020.121753
Received 12 July 2020; Received in revised form 10 September 2020; Accepted 22 September 2020
Available online 28 September 2020

It was found that La_2O_2S was a more efficient host than Y_2O_2S and Gd_2O_2S for all lanthanides. In this work, the luminescence spectra of only samples doped with Pr^{3+}, Eu^{3+}, Tb^{3+} ions are presented, and the quantum yield of luminophores and the studies of the luminescence kinetics presented in this work were not measured. Work [22] is devoted to the synthesis of $(Y_{1-x}Tm_x)_2O_2S$ and the study of its optical properties under laser excitation at 790 and 810 nm. The results obtained are of great practical importance, in that $(Y_{1-x}Tm_x)_2O_2S$ solid solutions are "invisible" IR phosphors and can be used in systems sensitive in a wide spectral range to create a new luminescence characteristic that allows excitation at 790 and 810 nm for reliable and reproducible identification of the phosphor by detecting strong emission bands of the Tm^{3+} ion in the range 785–825 nm at the afterglow stage. The synthesis of samples used in Ref. [22], described in Ref. [23], is multistage, laborious, and is of little use for obtaining optical materials in comparison with the method for obtaining luminophores proposed in this work. This article also does not describe research on the quantum yield of phosphors.

The method of obtaining new functional materials $RE_2O_2S:Ln^{3+}$ by sequential processing of powders of sulfates of rare-earth elements in a stream of H_2, H_2S, used in this work, has several advantages over solid-state synthesis methods. It is distinguished by manufacturability, productivity, the ability to produce batches of the product from tens to hundreds of grams and to conduct the process both continuously and interrupted at any time, without any significant negative consequences [24].

Thus, the aim of the work is to obtain solid solutions of oxysulfides by sequential processing of co-precipitated sulfates of rare-earth elements in an atmosphere of H_2, H_2S, and to study the morphology and optical properties of the obtained samples.

2. Materials and methods

2.1. Preparative methods

For the synthesis of $RE_2O_2S:Ln^{3+}$ compounds, calculated in a ratio of 95:5 mol. % of the amount of Ln_2O_3 (≥99.99%, ultrapure, OOO TDM-96, Russia). Oxide powders were weighed on an analytical balance to an accuracy of ±0.0001 g. Before weighing, the oxides were calcined in a muffle furnace at 900 °C for 24 h to remove sorbed water, as well as rare earth carbonates and hydroxides. Acids were selected using graduated pipettes with an accuracy of ±0.1 mL. Samples of oxides were poured into a heat-resistant glass with a capacity of 100 mL, then HNO_3 (Vekton Ltd., Russia) was poured with constant stirring, with a concentration of 15 mol/L, with a volume of 10 mL, if necessary, heated to a transparent state. The result was a mixture of nitrates:

$$0{,}95RE_2O_3 + 0{,}05Ln_2O_3 + 6HNO_3 \rightarrow 2(RE_{0,95}Ln_{0,05})(NO_3)_3 + 3H_2O \quad (1)$$

Then, nitrate solutions were cooled to a temperature of 35–40°C and 7 mL of H_2SO_4 (Vekton Ltd., Russia), with a concentration of 18 mol/L, with an excess of up to 7%, were added with a fine stream with constant stirring. As a result, crystalline hydrates of the precipitated co-crystallized sulfates were obtained according to the chemical reaction equation:

$$2(RE_{0.95}Ln_{0.05})(NO_3)_3 + 3H_2SO_4 + nH_2O \rightarrow (RE_{0.95}Ln_{0.05})_2(SO_4)_3{\cdot}nH_2O + 6HNO_3 \quad (2)$$

The resulting suspension was evaporated to dryness at 85–90 °C to remove water and nitrogen oxides, and then calcined at 600 °C for up to 12 h to release residual sulfuric acid and achieve high crystallinity of the sample. The method of co-precipitation of sulfates allows to achieve a uniform distribution of rare-earth metal cations. The resulting precipitate was triturated to obtain a powder and sieved through a sieve with a 100 μm cell.

The sample was treated in a hydrogen stream using the setup shown in Fig. S1. Hydrogen synthesis was performed using a SPECTR-6M hydrogen generator. Bidistilled water passed through a deionizer was used for electrolysis of water. A 10 g sulfate powder was placed in a quartz glass located in a reactor with a gas outlet tube placed in it. The device was carefully sealed and purged in a stream of hydrogen for 30 min in order to displace air from it with a gas flow rate of 7–8 L/h from the hydrogen generator, and then placed in a vertical furnace, setting the temperature mode using the Thermolux controller. After processing the sample for 1 h at 620 °C in a stream of H_2, the reactor was taken out of the furnace, cooled, and a sample was taken to study the phase composition. To complete the passage of chemical transformations, the treatment in a stream of hydrogen was carried out for up to 4 h (Fig. S1).

Processing in the H_2S stream was carried out in a similar way, only for the synthesis of hydrogen sulfide, an additional furnace was used, in which a reactor with sulfur (molten) melted at 400 °C was placed (Fig. S2). The formation of hydrogen sulfide occurred by the reaction:

$$H_2 + S \rightarrow H_2S \quad (3)$$

2.2. Physico-chemical analysis methods

X-ray phase analysis (XRD) was carried out on a BRUKER D2 PHASER diffractometer with a linear detector LYNXEYE (CuK_α radiation, Ni filter). Rietveld refinement of all samples was performed using TOPAS 4.2 [25]. All fixed reflexes of the obtained phases were indexed. The main refinement parameters are given in the supplementary materials (Tables S1 and S2).

Micrographs of powder particles from the processing steps in a stream of H_2, H_2S were obtained using a JEOL JSM-6510LV scanning electron microscope.

All photoluminescence measurements were carried out on a research grade spectrofluorometer Fluorolog-3 (Horiba Jobin Yvon) equipped with dual monochromators for excitation and emission channels and a 450 W xenon lamp as an excitation source. Lifetime measurements were performed at the same device using Xe-flash lamp (150 W power, 3 μs pulse width). The integration sphere (Quanta–φ, 6 inches) was used to measure the quantum yield. The measurements were carried out with powders according to the guide provided by manufacturer (four spectra-based measurement).

3. Results and discussions

The starting materials for the synthesis of solid solutions of oxysulfides are sulfates (Figs. 1a and 2 a), in which the doping ion is embedded in the host crystal. According to x-ray phase analysis, they are single-phase, which proves the formation of solid solutions of rare-earth sulfates.

For greater reliability, we trace the detailed formation of phases using the example of a sample of lanthanum-holmium sulfate. The appearance of gaseous reaction products at 610 °C allows processing in a stream of hydrogen at 620 °C for 1 h in order to draw up the equations of chemical reactions based on the results of X-ray phase analysis. As a result of processing, 4 phases were found in the powder composition: $(La_{0.95}Ho_{0.05})_2(SO_4)_3$ - $(La_{0.95}Ho_{0.05})_2O_2SO_4$ - $(La_{0.95}Ho_{0.05})_2O_2S$ – $La_{0.95}Ho_{0.05})_2O_3$ (Fig. 1b).

The same can be said about Fig. 2b; here, a similar phase composition is also observed, which is formed when the sample $Y_2(SO_4)_3:Tm^{3+}$ (5 mol. %) is processed in a hydrogen stream for 1 h at 620°C.

With an increase in the treatment time in the hydrogen stream to 4 h, at 620°C, two phases were detected in the sample: $(La_{0.95}Ho_{0.05})_2O_2S$ and $(La_{0.95}Ho_{0.05})_2O_3$ (Fig. 1c), as well as $(Y_{0.95}Tm_{0.05})_2O_2S$ and $(Tm_{0.95}Ho_{0.05})_2O_3$ in Fig. 2c.

The following chemical equations correspond to the formation of the corresponding reduction products:

$$(RE_{0.95}Ln_{0.05})_2(SO_4)_3 + 6H_2 \rightarrow (RE_{0.95}Ln_{0.05})_2O_2SO_4 + 2S + 6H_2O \quad (4)$$

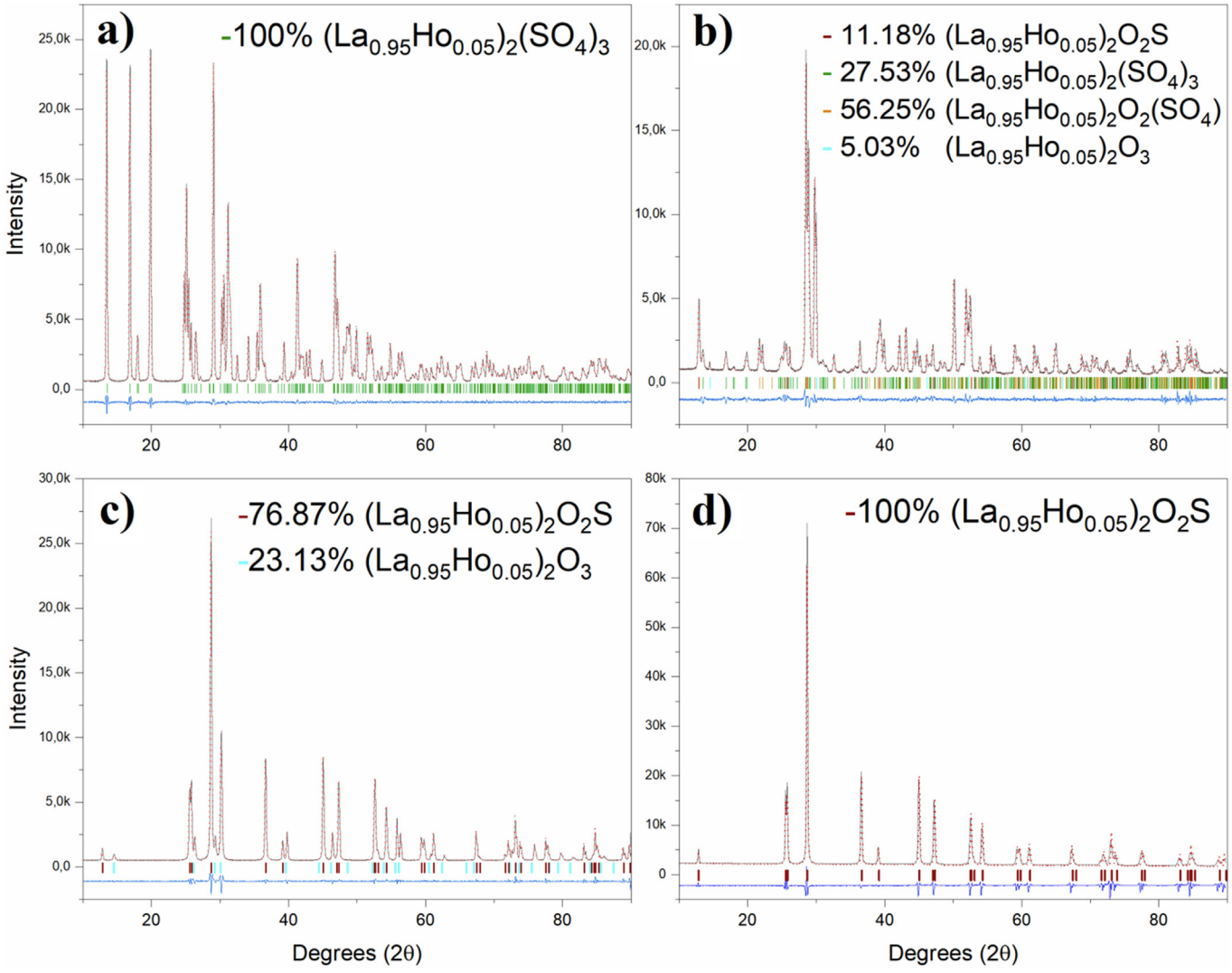

Fig. 1. Difference Rietveld plot of: a) $(La_{0.95}Ho_{0.05})_2(SO_4)_3$; b) $(La_{0.95}Ho_{0.05})_2(SO_4)_3$-$(La_{0.95}Ho_{0.05})_2O_2SO_4$-$(La_{0.95}Ho_{0.05})_2O_2S$-$(La_{0.95}Ho_{0.05})_2O_3$; c) $(La_{0.95}Ho_{0.05})_2O_2S$-$(La_{0.95}Ho_{0.05})_2O_3$; d) $(La_{0.95}Ho_{0.05})_2O_2S$.

$$(RE_{0.95}Ln_{0.05})_2(SO_4)_3 + 10H_2 \rightarrow (RE_{0.95}Ln_{0.05})_2O_2S + 2S + 10H_2O \quad (5)$$

$$(RE_{0.95}Ln_{0.05})_2(SO_4)_3 + 5H_2 \rightarrow (RE_{0.95}Ln_{0.05})_2O_3 + 2SO_2 + 5H_2O \quad (6)$$

$$(RE_{0.95}Ln_{0.05})_2O_2SO_4 + 4H_2 \rightarrow (RE_{0.95}Ln_{0.05})_2O_2S + 4H_2O \quad (7)$$

After 4 h of carrying out the process at this temperature, according to x-ray phase analysis, the polycrystalline products consist of two phases: $(RE_{0.95}Ln_{0.05})_2O_2S$, $(RE_{0.95}Ln_{0.05})_2O_3$ (Figs. 1c and 2c). In the products of intermediate transformations there are no compounds containing SO_4^{2-} ions, which indicates the complete occurrence of the redox reaction. It should be noted that the content of the by-product, which is oxide, in the case of the reduction of yttrium sulfates is much higher (40.91 mol. %) than the corresponding compounds with lanthanum (23.13 mol.%). The thermodynamic stability of La_2O_2S is higher than that of Y_2O_2S, and that of Y_2O_3 is higher than that of La_2O_3 [26]. This may be another reason for the benefits of reaction 6.

Thus, during the reduction of rare earth sulfates in a hydrogen atmosphere for 4 h, two-phase polycrystalline intermediate products are formed with a predominant content of the oxysulfide phase, which greatly facilitated the further sulfidation procedure.

A further, final step in the synthesis is the sulfidation reaction in an H_2S atmosphere. After processing the mixture of oxysulfide and oxide in a stream of hydrogen sulfide at 1000 °C for 4 h, according to the X-ray phase analysis, a single-phase sample of a solid solution of oxysulfide with the general formula $(RE_{0.95}Ln_{0.05})_2O_2S$ is fixed (Figs. 1d and 2d):

$$(RE_{0.95}Ln_{0.05})_2O_3 + H_2S \rightarrow (RE_{0.95}Ln_{0.05})_2O_2S + H_2O \quad (8)$$

The calcined powder of sulfate $(La_{0.95}Tm_{0.05})_2(SO_4)_3$, according to the data of scanning electron microscopy (Fig. 3 a), consists of grains of various shapes with average sizes (5−10) × (10–30) μm. Fragments of a dense layered structure alternate with the resulting voids. The course of chemical reactions changes the morphology of the particles of the starting compounds. In the process of successive exposure to H_2 at 620 °C, 4 h, H_2S at 1000 °C, 4 h, a single-phase sample of oxysulfide $(La_{0.95}Tm_{0.05})_2O_2S$ is formed, while most of the particles form a faceting, indicating the formation of a compound with a hexagonal syngony with angles of 60° and 120°. Thermal action of gaseous reagents H_2, H_2S on sulfates leads to heterogeneous reactions of thermal dissociation and the formation of new phases. Fig. 4b shows $(La_{0.95}Tm_{0.05})_2O_2S$ particles, when compared with the initial compound, a much larger number of particles with sizes of 0.5–1 μm can be noted, but the agglomerate nature of particles from 5 to 30 μm is also preserved. The morphological transformation of particles is obviously associated with the thermal effect of gaseous reagents and the occurrence of diffusion processes during reduction and sulfidation.

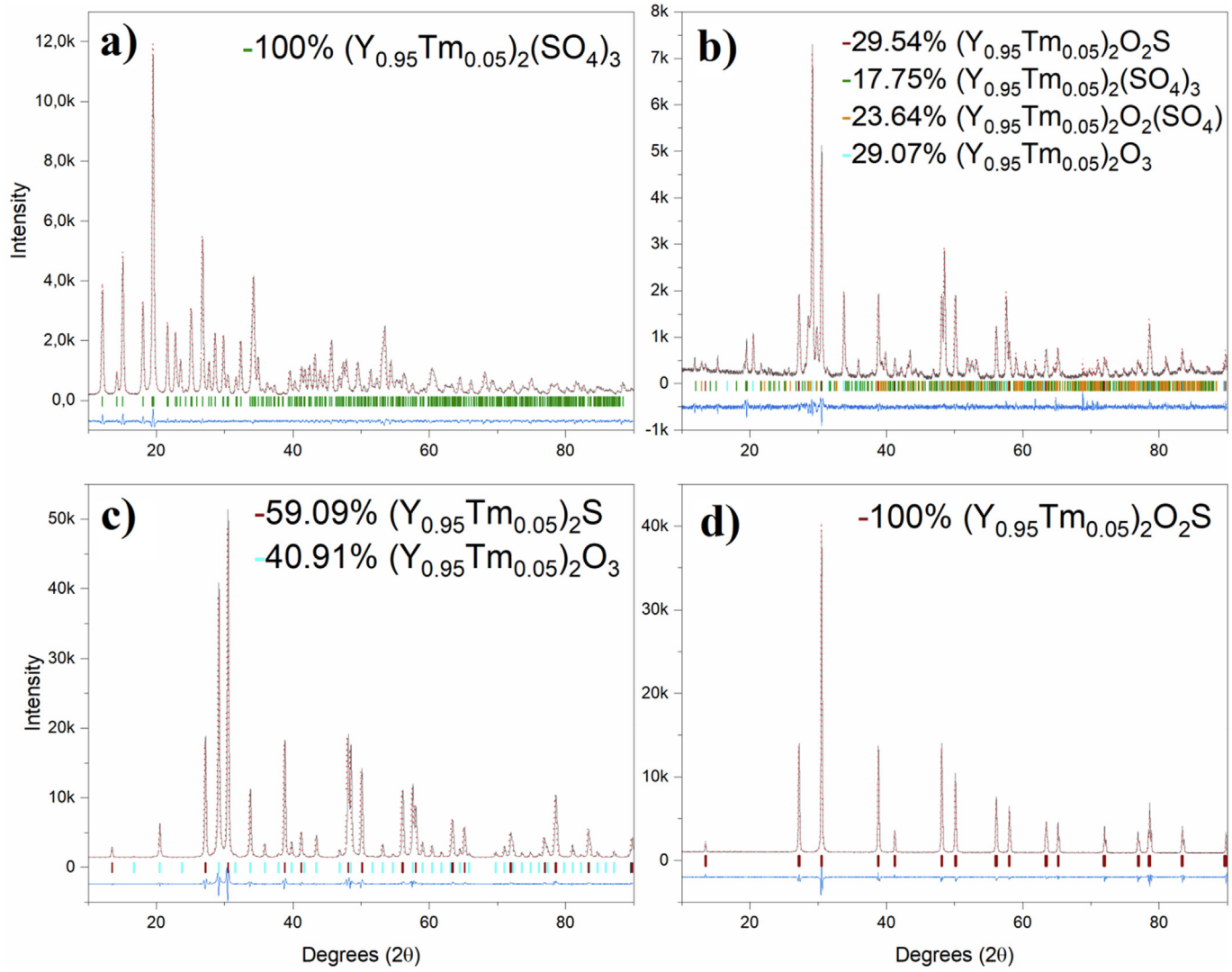

Fig. 2. Difference Rietveld plot of: a) $(Y_{0.95}Tm_{0.05})_2(SO_4)_3$; b) $(Y_{0.95}Tm_{0.05})_2(SO_4)_3$-$(Y_{0.95}Tm_{0.05})_2O_2SO_4$-$(Y_{0.95}Tm_{0.05})_2O_2S$-$(Y_{0.95}Tm_{0.05})_2O_3$; c)$(Y_{0.95}Tm_{0.05})_2O_2S$-$(Y_{0.95}Tm_{0.05})_2O_3$; d) $(Y_{0.95}Tm_{0.05})_2O_2S$.

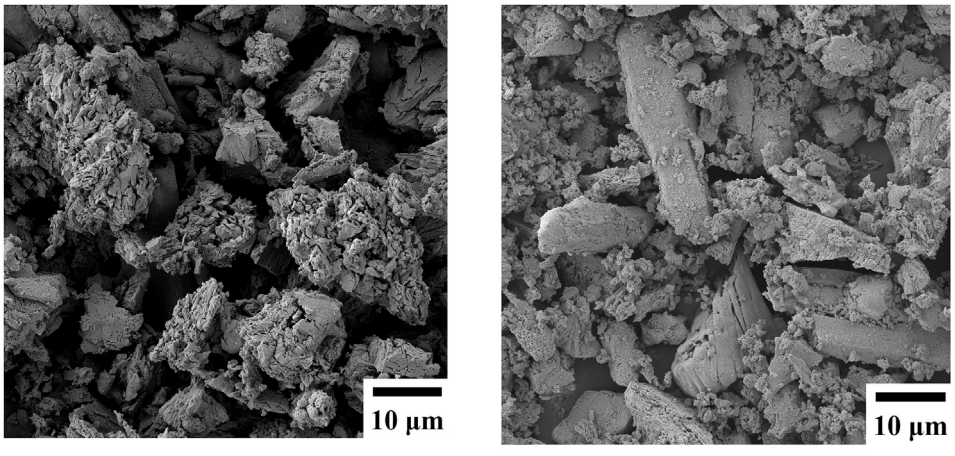

Fig. 3. SEM images of a) $(La_{0.95}Tm_{0.05})_2(SO_4)_3$; b) $(La_{0.95}Tm_{0.05})_2O_2S$.

The excitation and emission spectra of $(Y_{0.95}Ho_{0.05})_2O_2S$ phosphor are presented in Fig. 4a and 4b. Emission spectrum of $(Y_{0.95}Ho_{0.05})_2O_2S$ powder obtained upon 462 nm excitation consists of typical narrow lines which can be assigned to following 4f-4f transitions: $^5F_3$–$^5I_8$ (491 nm),

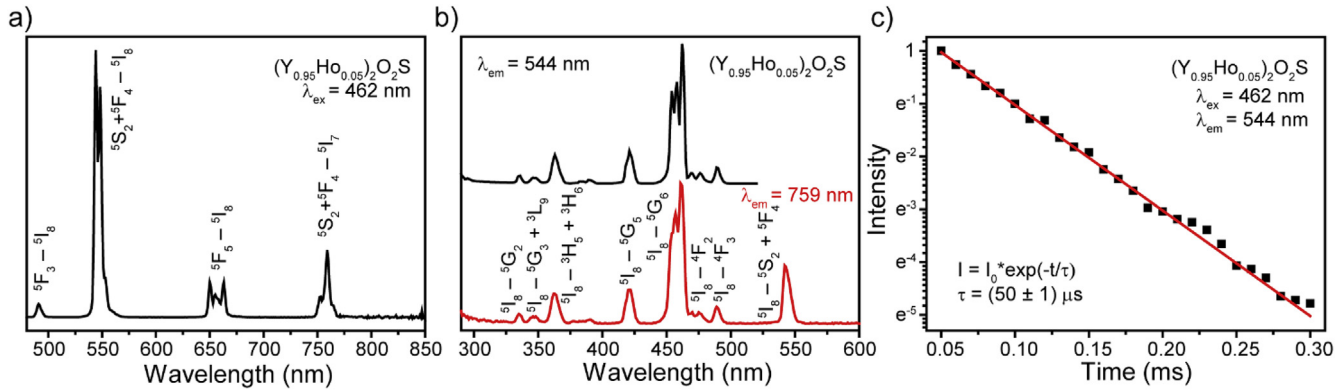

Fig. 4. a) Emission spectrum ($\lambda_{ex} = 462$ nm), b) excitation spectra ($\lambda_{em} = 544$ nm and 759 nm) and c) luminescence decay of $(Y_{0.95}Ho_{0.05})_2O_2S$ powder.

$^5S_2+^5F_4-^5I_8$ (544 and 548 nm), $^5F_5-^5I_8$ (650, 655 and 663 nm) and $^5S_2+^5F_4-^5I_7$ (753 and 759 nm) [27,28]. Majority of emission bands include several lines because of Stark splitting of energy levels. Excitation spectra of $(Y_{0.95}Ho_{0.05})_2O_2S$ powder were measured for two transitions: $^5S_2+^5F_4-^5I_8$ (544 nm) and $^5S_2+^5F_4-^5I_7$ (759 nm). Spectral line positions did not depend on monitoring wavelength. Better resolution in the first case is explained by less spectral slit width. The observed excitation lines correspond to $^5I_8-^5G_2$ (336 nm), $^5I_8-^5G_3+^3L_9$ (347 nm), $^5I_8-^3H_5+^3H_6$ (363 nm), $^5I_8-^5G_4$ (383 and 390 nm), $^5I_8-^5G_5$ (421 nm), $^5I_8-^5G_6$ (454, 458 and 462 nm), $^5I_8-^4F_2$ (470, 477 nm), $^5I_8-^4F_3$ (490 nm), $^5I_8-^5S_2+^5F_4$ (542 nm) [29,30]. Fig. 4c displays luminescence decay curve of $(Y_{0.95}Ho_{0.05})_2O_2S$ sample measured at the most prominent transition ($\lambda_{ex} = 462$ nm, $\lambda_{em} = 544$ nm). It is clearly seen, that the experimental data demonstrate single exponential behavior:

$$I = A \cdot e^{-\frac{t}{\tau}} \quad (9)$$

where τ is observed lifetime. The observed lifetime of $^5S_2+^5F_4$ excited level was found to be (50 ± 1) μs.

To study host composition effect on photoluminescence properties, we regarded $(La_{0.95}Ho_{0.05})_2O_2S$ sample. Y_2O_2S and La_2O_2S have similar structure and symmetry, the only difference is substitution of yttrium (r = 89 p.m.) to lanthanum (r = 102 p.m.) ions. Both hosts have the trigonal space group D^3_{3d} and the point symmetry of the doping ion is C_{3v}. The crystal structure parameters of studied oxysulfides differ in such a way that La_2O_2S has the larger interionic distances than Y_2O_2S one [21]. Emission spectrum of $(La_{0.95}Ho_{0.05})_2O_2S$ powder exhibited bands similar to those observed in case of $(Y_{0.95}Ho_{0.05})_2O_2S$ sample: $^5F_3-^5I_8$ (490 nm), $^5S_2+^5F_4-^5I_8$ (544 and 547 nm), $^5F_5-^5I_8$ (650, 653 and 660 nm) and $^5S_2+^5F_4-^5I_7$ (751 and 757 nm) (Fig. 5a). Small blue shift of lines and redistribution between them were observed. The observed spectral shift can be explained as follows: as the interionic distances increase, the energy levels of doping ions tend to approach the energy levels of a free ion [21]. We monitored excitation spectra of $(La_{0.95}Ho_{0.05})_2O_2S$ phosphor for $^5S_2+^5F_4-^5I_8$ (544 nm) and $^5S_2+^5F_4-^5I_7$ (757 nm) transitions (Fig. 5b). Both spectra are dominated by $^5I_8-^5G_6$ transition (454, 457 and 461 nm). Almost all excitation bands also demonstrated aforementioned blue shift. Luminescence kinetics of $(La_{0.95}Ho_{0.05})_2O_2S$ sample was measured at the most intensive line centered at 544 nm upon 461 nm excitation (Fig. 5c). Single exponential fitting of decay curve allowed to obtain $^5S_2+^5F_4$ lifetime for $(La_{0.95}Ho_{0.05})_2O_2S$ of (103 ± 2) μs.

Fig. 6a shows emission spectrum of $(Y_{0.95}Tm_{0.05})_2O_2S$ sample upon 363 nm excitation measured within spectral range of 400–850 nm. It displays narrow bands assigned to the 4f-4f transitions, which are centered at 457 nm ($^1D_2-^3F_4$), 666 and 673 nm ($^1G_4-^3F_4$), 760 nm ($^3F_{2,3}-^3H_6$) and 789, 800, 813 nm ($^3H_4-^3H_6$) [31–33]. Low-intensity bands near 550 nm are most probably attributed to the emission of Er^{3+} impurity ions situated in the sample. As luminescence of Tm^{3+} ions in Y_2O_2S is quite weak, we have also observed broad host emission situated in the 400–550 nm spectral region. Excitation spectra of $(Y_{0.95}Tm_{0.05})_2O_2S$ phosphor were monitored at two transitions: $^1D_2-^3F_4$ (457 nm) and $^3H_4-^3H_6$ (800 nm). Contrary to Ho^{3+}-doped samples, we measured excitation spectra for transitions originated from different excited levels: $^1D_2$ and $^3H_4$, respectively. These spectra consist of sharp lines corresponding to intra-configurational f-f transitions: $^3H_6-^1D_2$ (363 nm), $^3H_6-^1G_4$ (468 nm) and $^3H_6-^3F_{2,3}$ (694 nm) [31–33]. Noteworthy, $^3H_6-^1D_2$ transition presented on both spectra had the same spectral position. We monitored luminescence decay curve of $(Y_{0.95}Tm_{0.05})_2O_2S$ powder for the most intense transition – $^1D_2-^3F_4$. Experimental data were fitted with single exponential decay with sufficient accuracy (Adj. $R^2 = 0.984$). The observed $^1D_2$ lifetime was determined to be (6.5 ± 0.3) μs.

The steady state luminescence spectra and luminescence kinetics of $(La_{0.95}Tm_{0.05})_2O_2S$ phosphor are presented in Fig. 7. Host change led to

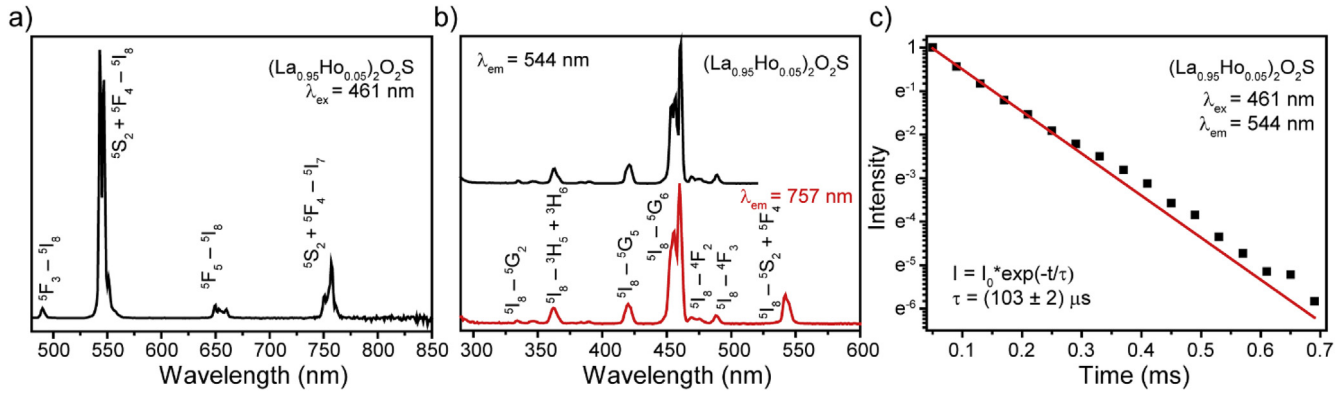

Fig. 5. a) Emission spectrum ($\lambda_{ex} = 461$ nm), b) excitation spectra ($\lambda_{em} = 544$ nm and 757 nm) and c) luminescence decay of $(La_{0.95}Ho_{0.05})_2O_2S$ powder.

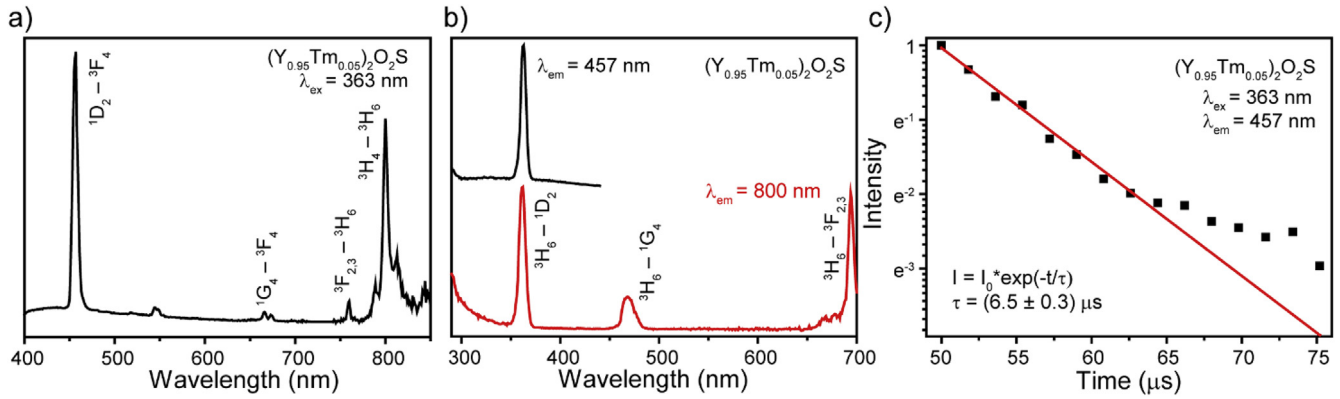

Fig. 6. a) Emission spectrum ($\lambda_{ex} = 363$ nm), b) excitation spectra ($\lambda_{em} = 457$ nm and 800 nm) and c) luminescence decay of $(Y_{0.95}Tm_{0.05})_2O_2S$ powder.

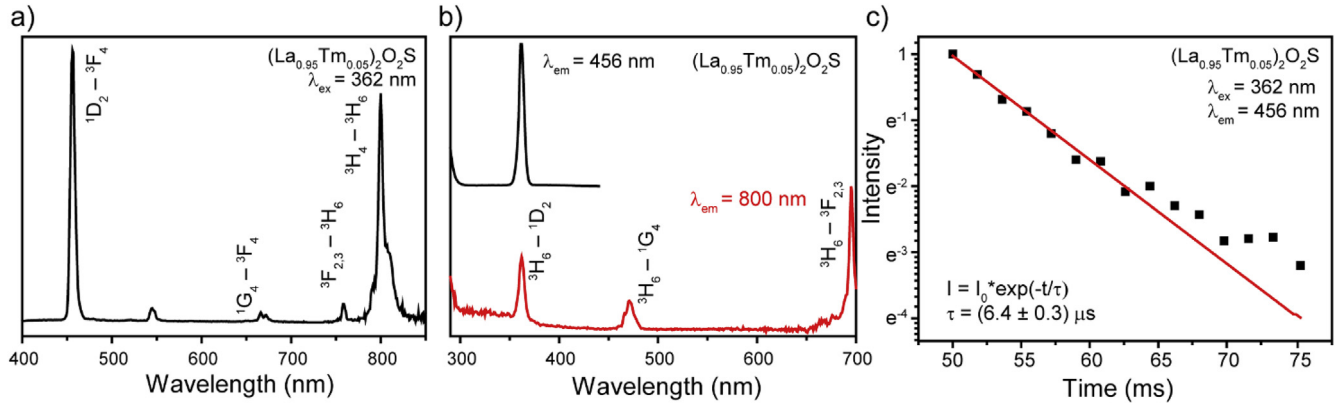

Fig. 7. a) Emission spectrum ($\lambda_{ex} = 362$ nm), b) excitation spectra ($\lambda_{em} = 456$ nm and 800 nm) and c) luminescence decay of $(La_{0.95}Tm_{0.05})_2O_2S$ powder.

the insignificant blue shift of spectral lines and intensity redistribution. Emission spectrum includes $^1D_2$–$^3F_4$ (456 nm), $^1G_4$–$^3F_4$ (666 and 672 nm), $^3F_{2,3}$–$^3H_6$ (758 nm) and $^3H_4$–$^3H_6$ (800 nm) transitions. Excitation spectrum consists of $^3H_6$–$^1D_2$ (362 nm), $^3H_6$–$^1G_4$ (471 nm) and $^3H_6$–$^3F_{2,3}$ (695 nm) transitions. Luminescence decay curve of $^1D_2$–$^3F_4$ transition presented single exponential behavior, and $^1D_2$ lifetime was found to be (6.4 ± 0.3) μs.

An important parameter of phosphor is quantum yield (**φ**), which shows conversion efficiency of absorbed photons into emitted ones. We measured quantum yield of synthesized powders via absolute technique using integrating sphere. The obtained **φ** values as well as previously obtained photoluminescence characteristics are summarized in Table 1. The best quantum yield of about 12% was found for $(La_{0.95}Ho_{0.05})_2O_2S$ sample. Analyzing obtained experimental results, we can conclude that La_2O_2S is better host for holmium and thulium doping compared with Y_2O_2S. The same situation was observed for other lanthanides in these oxysulfide hosts [21].

Possible application of synthesized powders as a phosphor was studied via photometric characterization. The Commission Internationale de L'Eclairage (CIE) chromaticity coordinates calculated from measured emission spectra are listed in Table 1 and presented in Fig. 8. Despite small spectral shift of emission lines in Y_2O_2S and La_2O_2S doped samples, chromaticity coordinates vary significantly. Such behavior is elucidated by considerable intensity redistribution between emission lines. Noteworthy, chromaticity coordinates of $(La_{0.95}Ho_{0.05})_2O_2S$ and $(La_{0.95}Tm_{0.05})_2O_2S$ samples are close to green (0.300, 0.600) and blue (0.150, 0.060) colors – most commonly used primary colors for display monitors and TV's (ITU-R BT.709 standard primaries). It makes synthesized powders suitable for efficient green and blue phosphors application.

Table 1
Main emission lines (λ_{em}), lifetime (**τ**), quantum yield (**φ**) and CIE1931 chromaticity coordinates of $RE_2O_2S:Ln^{3+}$ samples.

Material	λ_{em}, nm	τ, μs	φ, %	CIE1931 chromaticity coordinates
$(Y_{0.95}Ho_{0.05})_2O_2S$	491, 544, 663, 759	50 ± 1	2.7	(0.296, 0.684)
$(La_{0.95}Ho_{0.05})_2O_2S$	490, 544, 650, 757	103 ± 2	12.3	(0.278, 0.704)
$(Y_{0.95}Tm_{0.05})_2O_2S$	457, 544, 666, 760, 800	6.5 ± 0.3	0.1	(0.189, 0.133)
$(La_{0.95}Tm_{0.05})_2O_2S$	456, 545, 666, 758, 800	6.4 ± 0.3	0.3	(0.171, 0.083)

4. Conclusion

The sequence of phase formation of sulfates doped with rare earth elements ($(La_{0.95}Ln_{0.05})_2(SO_4)_3$ and $(Y_{0.95}Ln_{0.05})_2(SO_4)_3$ (Ln = Ho^{3+}, Tm^{3+})) was studied during their sequential processing in a stream of H_2, H_2S. The phase and morphological certification of the obtained solid solutions of rare earth oxysulfides were carried out. Excitation and emission spectra of $La_2O_2S:Ln^{3+}$ и $Y_2O_2S:Ln^{3+}$ (Ln^{3+} = Ho, Tm) included characteristic narrow bands corresponding to the 4f-4f intra-configurational transitions. Change of Y_2O_2S host to La_2O_2S resulted in small blue shift of emission lines which is caused by the larger interionic distances in the latter case. Study of luminescence decay showed that Ho^{3+}-doped La_2O_2S powder had twice bigger lifetime compared with Ho^{3+}-doped Y_2O_2S one, whereas Tm^{3+}-doped samples have similar lifetime independently on host. The best quantum yield of about 12% was found for $La_2O_2S:Ho^{3+}$ sample. Chromaticity coordinates of Ho^{3+}

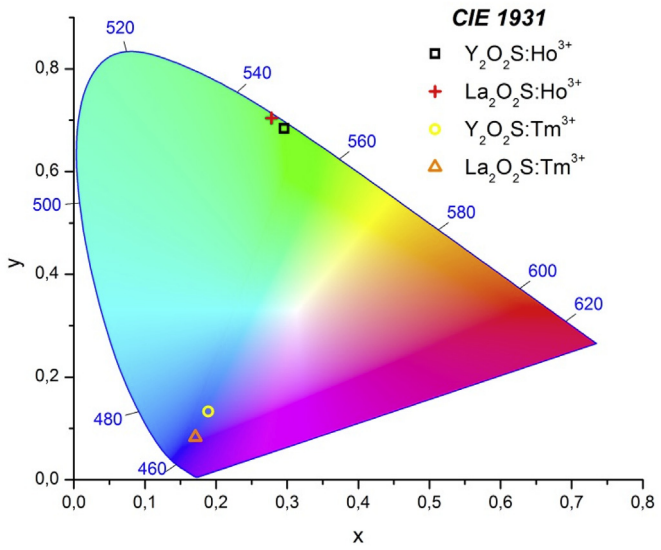

Fig. 8. CIE1931 chromaticity coordinates of synthesized samples.

and Tm^{3+}-doped La_2O_2S powders were close to green and blue standard colors, which makes them perspective for phosphor applications.

CRediT authorship contribution statement

E.I. Sal'nikova: Conceptualization, Methodology, Resources, Investigation. **Yu.G. Denisenko:** Data curation, Writing - original draft, Validation. **I.E. Kolesnikov:** Visualization, Writing - original draft. **E. Lähderanta:** Validation, Visualization. **O.V. Andreev:** Supervision, Project administration. **N.O. Azarapin:** Formal analysis, Investigation. **S.A. Basova:** Writing - review & editing. **A.A. Gubin:** Formal analysis, Investigation. **A.S. Oreshonkov:** Validation, Project administration.

Declaration of competing interest

The authors declare that they have no known competing financial interests or personal relationships that could have appeared to influence the work reported in this paper.

Acknowledgments

Photoluminescence measurements were performed in "Center for Optical and Laser materials research" (St. Petersburg State University).

Appendix A. Supplementary data

Supplementary data to this article can be found online at https://doi.org/10.1016/j.jssc.2020.121753.

References

[1] E.I. Sal'nikova, Yu.G. Denisenko, A.S. Aleksandrovsky, I.E. Kolesnikov, E. Lähderanta, P.O. Andreev, N.O. Azarapin, O.V. Andreev, S.A. Basova, A.V. Matigorov, Synthesis and optical properties RE_2O_2S:Ln (RE = La, Y; Ln = Ce, Eu, Dy, Er), J. Solid State Chem. 279 (2019), https://doi.org/10.1016/j.jssc.2019.120964, 120964. 1-6.

[2] Yu.G. Denisenko, E.I. Sal'nikova, S.A. Basova, M.S. Molokeev, A.S. Krylov, A.S. Aleksandrovsky, A.S. Orechenkov, V.V. Atuchin, S.S. Volkova, N.A. Khritokhin, O.V. Andreev, Synthesis of samarium oxysulfate $Sm_2O_2SO_4$ in the high-temperature oxidation reaction and its structural, thermal and luminescent properties, Molecules 25 (2020) 1330. 1–1330.15, https://doi.org/10.3390/molecules25061330.

[3] Yu.G. Denisenko, M.S. Molokeev, A.S. Krylov, A.S. Alecsandrovsky, A.S. Oreshonkov, V.V. Atuchin, N.O. Azarapin, P.E. Plyusnin, E.I. Sal'nikova, O.V. Andreev, High-temperature oxidation of europium (II) sulfide, J. Ind. Eng. Chem. 79 (2019) 62–70, https://doi.org/10.1016/j.jiec.2019.05.006.

[4] P.O. Andreev, E.I. Sal'nikova, O.V. Andreev, YuG. Denisenko, I.M. Kovenskii, Synthesis and upconversion luminescence spectra of $(Y_{1-x-y}Yb_xEr_y)_2O_2S$, Inorg. Mater. 53 (2) (2017) 200–206, https://doi.org/10.1134/S0020168517020029.

[5] S.W. Kim, T. Hasegawa, T. Abe, H. Nakagawa, S. Hasegawa, K. Seki, K. Toda, K. Uematsu, T. Ishigaki, M. Sato, Abnormal improvement in emission of lanthanum oxysulfide phosphor $La_2O_2S:Tb^{3+}$ synthesized by a novel method, thermal decomposition in eutectic molten salt, Ceramic Int. 42 (2016) 10389–10392, https://doi.org/10.1016/j.ceramint.2016.03.176.

[6] Y. Yang, C. Mi, F. Yu, C. Guo, G. Li, J. Zhang, L. Liu, Y. Liu, X. Li, Optical thermometry based on the upconversion fluorescence from Yb^{3+}/Er^{3+} codoped La_2O_2S phosphor, Ceramic Int. 40 (7) (2014) 9875–9880, https://doi.org/10.1016/j.ceramint.2014.02.081.

[7] I.A. Razumkova, Synthesis of $NaYF_4$ compounds from sulfide precursors, J. Fluor. Chem. 205 (2018) 1–4, https://doi.org/10.1016/j.jfluchem.2017.10.012.

[8] I.A. Razumkova, Yu.G. Denisenko, A.N. Boyko, D.A. Ikonnikov, A.S. Aleksandrovsky, N.O. Azarapin, O.V. Andreev, Synthesis and upconversion luminescence in LaF_3: Yb^{3+}, Ho^{3+}, $GdF_3:Yb^{3+}$, Tm^{3+} and $YF_3:Yb^{3+}$, Er^{3+} obtained from sulfide precursors, Z. Anorg. Allg. Chem. 645 (2019) 1393–1401, https://doi.org/10.1002/zaac.201900204.

[9] I.E. Kolesnikov, E.V. Golyeva, E. Lähderanta, A.V. Kurochkin, M.D. Mikhailov, Ratiometric thermal sensing based on Eu^{3+}-doped YVO_4 nanoparticles, J. Nanoparticle Res. 18 (12) (2016) 354, https://doi.org/10.1007/s11051-016-3675-8.

[10] I.E. Kolesnikov, A.A. Kalinichev, M.A. Kurochkin, D.V. Mamonova, E.Yu Kolesnikov, A.V. Kurochkin, E. Lähderanta, M.D. Mikhailov, Y2O3:Nd3+ nanocrystals as ratiometric luminescence thermal sensors operating in the optical windows of biological tissues, J. Lumin. 204 (2018) 506–512, https://doi.org/10.1016/j.jlumin.2018.08.050.

[11] G. Jiang, X. Wei, Y. Chen, C. Duan, M. Yin, B. Yang, W. Cao, Luminescent $La_2O_2S:Eu^{3+}$ nanoparticles as non-contact optical temperature sensor in physiological temperature range, Mater. Lett. 143 (2015) 98–100, https://doi.org/10.1016/j.matlet.2014.12.057.

[12] M. Aryal, S.W. Allison, K. Olenick, F. Sabri, Flexible thin film ceramics for high temperature thermal sensing applications, Opt. Mater. 100 (109656) (2020) 1–11, https://doi.org/10.1016/j.optmat.2020.109656.

[13] S. Tan, D. Li, Enhancing oxygen storage capability and catalytic activity of lanthanum oxysulfide (La_2O_2S) nanocatalysts by sodium-and iron/sodium-doping, ChemCatChem 10 (2018) 550–558, https://doi.org/10.1002/cctc.201701117.

[14] W. Zhang, I.W.C.E. Arends, K. Djanashvili, Nanoparticles of oxysulfate/oxysulfide for improved oxygen storage/release, Dalton Trans. 45 (2016) 14019–14022, https://doi.org/10.1039/C6DT01667G.

[15] T.W. Chou, S. Mylswamy, R.S. Liu, S.Z. Chuang, Eu substitution and particle size control of Y_2O_2S for the excitation by UV light emitting diodes, Solid State Commun. 136 (2005) 205–209, https://doi.org/10.1016/j.ssc.2005.07.032.

[16] P. Han, Y. Zhu, J. Li, T. Li, X. Jiang, C. Zhang, B. Jiao, Q. Wu, Upconversion white light output in $(Y_{0.9}Gd_{0.1})_2O_2S$ matrix tri-doped with $Yb^{3+}/Tm^{3+}/Er^{3+}$ or $Yb^{3+}/Tm^{3+}/Ho^{3+}$, Nanosci. Nanotechnol. Lett. 9 (4) (2017) 586–591, https://doi.org/10.1166/nnl.2017.2361.

[17] G. Ajithkumar, B. Yoo, D.E. Goral, P.J. Hornsby, A.L. Lin, U. Ladiwala, V.P. Dravide, D.K. Sardara, Multimodal bioimaging using a rare earth doped Gd_2O_2S:Yb/Er phosphor with upconversion luminescence and magnetic resonance properties, J. Mater. Chem. B. 1 (2013) 1561–1572, https://doi.org/10.1039/c3tb00551h.

[18] Q. Ju, D. Tu, Y. Liu, H. Zhu, X. Chen, Lanthanide-doped inorganic nanocrystals as luminescent biolabels, Comb. Chem. High Throughput Screen. 15 (7) (2012) 580–594, https://doi.org/10.2174/138620712801619177.

[19] X. Wang, Z. Hu, Q. Zhu, J. Li, X. Sun, $La_2O_2SO_4$:RE/Yb new phosphors for near infrared to visible and near infrared upconversion luminescence (RE=Ho, Er, Tm), J. Am. Ceram. Soc. 101 (7) (2018) 2701–2706, https://doi.org/10.1111/jace.15477.

[20] S.A. Osseni, S. Lechevallier, M. Verelst, P. Perriat, J. Dexpert-Ghys, D. Neumeyer, R. Garcia, F. Mayer, K. Djanashvili, J.A. Peters, E. Magdeleine, H. Gros-Dagnac, P. Celsis, R. Mauricot, Gadolinium oxysulfide nanoparticles as multimodal imaging agents for T_2-weighted MR, X-ray tomography and photoluminescence, Nanoscale 6 (2014) 555–564, https://doi.org/10.1039/C3NR03982J.

[21] H. Ratinen, X-Ray-Excited optical fluorescence of ten rare earth ions in Y_2O_2S, La_2O_2S, and Gd_2O_2S, Phys. Status Solidi 12 (1972) 447–451, https://doi.org/10.1002/pssa.2210120211.

[22] O.Ya Manashirov, A.N. Georgobiani, V.B. Gutan, et al., Synthesis and IR-excited luminescence of $(Y_{1-x}Tm_x)_2O_2S$ solid solutions/, Inorg. Mater. 49 (3) (2013) 278–282, https://doi.org/10.1134/S0020168513020131.

[23] O. Ya, Manashirov, AntiStokes phosphors for visual ization of weak IR fields in the range 1.4–1.7 μm: 1. Structural and kinetic studies of the formation of Rare Earth oxysulfide based phosphors, Sb. Nauchn. Tr. NPF Lyuminofor. 43 (1999) 42–65.

[24] A.O. Semiyou, YuG. Denisenko, J.K. Fatombi, E.I. Sal'nikova, O.V. Andreev, Synthesis and characterization of $Ln_2O_2SO_4$ (Ln = Gd, Ho, Dy and Lu) nanoparticles obtained by coprecipitation method and study of their reduction reaction under H_2 flow, J. Nanostuct. Chem. 7 (2017) 337–343, https://doi.org/10.1007/s40097-017-0243-4.

[25] Bruker AXS TOPAS V4, General Profile and Structure Analysis Software for Powder Diffraction Data. User's Manual, Bruker AXS, Karlsruhe, Germany, 2008.

[26] Y.L. Suponitskiy, Thermal Chemistry of Oxygen-Containing Compounds of REE Elements and Elements of Group VI, Thesis of Doctor of Science in Chemistry, D. Mendeleev University of Chemical Technology of Russia, Moscow, Russia, 2002.

[27] L. Guo, Yu Wang, J. Zhang, Y. Wang, P. Dong, Near-infrared quantum cutting in Ho^{3+}, Yb^{3+}-codoped $BaGdF_5$ nanoparticles via first-and second-order energy transfers,

Nanoscale Res Lett 7 (1) (2012) 1–7, https://doi.org/10.1186/1556-276X-7-636, 636.

[28] B. Suresh, Ya Zhydachevskii, M.G. Brik, A. Suchocki, M. Srinivasa Reddy, M. Piasecki, N. Veeraiah, Amplification of green emission of Ho^{3+} ions in lead silicate glasses by sensitizing with Bi^{3+} ions, J. Alloys Compd. 683 (2016) 114–122, https://doi.org/10.1016/j.jallcom.2016.05.056.

[29] N.S. Hussain, N. Ali, A.G. Dias, M.A. Lopes, J.D. Santos, S. Buddhudu, Absorption and emission properties of Ho^{3+} doped lead–zinc–borate glasses, Thin Solid Films 515 (1) (2006) 318–325, https://doi.org/10.1016/j.tsf.2005.12.085.

[30] C.R. Kesavulu, H.J. Kim, S.W. Lee, J. Kaewkhao, N. Wantana, S. Kothan, S. Kaewjaeng, Optical spectroscopy and emission properties of Ho3 +-doped gadolinium calcium silicoborate glasses for visible luminescent device applications, J. Non-Cryst. Solids 474 (2017) 50–57, https://doi.org/10.1016/j.jnoncrysol.2017.08.018.

[31] O.A. Lopez, J. McKittrick, L.E. Shea, Fluorescence properties of polycrystalline Tm^{3+} - activated $Y_3Al_5O_{12}$ in the visible and near IR ranges, J. Lumin. 71 (1997) 1–11, https://doi.org/10.1016/S0022-2313(96)00123-8.

[32] J.X. Lefu, M.J. Deng, H. Liu, B. Ma, M. Guan, L. Liao, G. Lv, Up-conversion luminescence properties and energy transfer of Tm^{3+}/Yb^{3+} co-doped $BaLa_2ZnO_5$, J. Solid State Chem. 231 (2015) 212–216, https://doi.org/10.1016/j.jssc.2015.07.046Get rights and content.

[33] I.E. Kolesnikov, M.A. Kurochkin, A.A. Kalinichev, E.Yu Kolesnikov, E. Lähderanta, Optical temperature sensing in Tm^{3+}/Yb^{3+}-doped GeO_2-PbO-PbF_2 glass ceramics based on ratiometric and spectral line position approaches, Sensors and Actuators A: Phys. 284 (2018) 251–259, https://doi.org/10.1016/j.sna.2018.10.039.